steel research international

steel research international

RESEARCH ARTICLE OPEN ACCESS

Influence of an Electromagnetic Field on Direct Reduction of Iron Oxide Using Hydrogen as a Reducing Agent

Mykyta Levchenko[1] | Oleksandr Gryshyn[2] | Oleksandr Velychko[2] | Oleksandr Grek[2] | Anzhela Nadtochiy[2] | Olena Volkova[1]

[1]Institute of Iron and Steel Technology, TU Bergakademie Freiberg, Freiberg, Germany | [2]Dnipro Metallurgical Institute, Ukrainian State University of Science and Technologies, Dnipro, Ukraine

Correspondence: Mykyta Levchenko (Mykyta.Levchenko@iest.tu-freiberg.de)

Received: 13 October 2025 | **Revised:** 26 January 2026 | **Accepted:** 28 January 2026

Keywords: direct reduction | direct reduced iron | electromagnetic field | hydrogen | iron oxide

ABSTRACT

This work investigates the effect of electromagnetic fields (EMF) of varying frequencies on the reduction process of iron oxides and industrial iron ore in a hydrogen atmosphere using thermogravimetric analysis. Both extremely low-frequency (50 Hz) and middle-frequency (25 kHz) EMFs were found to increase the reduction degree and accelerate the reduction reaction compared with experiments without EMF. The application of extremely low-frequency EMF did not cause additional thermal heating of investigated samples. However, with middle-frequency EMF, heating of charged material was observed, which was effectively compensated for by the furnace's automatic power regulation. Experiments with industrial iron ore confirmed that EMF application had a positive effect on reduction process even above the Curie temperature, indicating that the effect is not governed by magnetic properties of iron. These findings demonstrate that EMF-assisted hydrogen reduction can enhance reaction kinetics and reduce hydrogen consumption, offering a promising pathway toward more energy-efficient and sustainable steelmaking.

1 | Introduction

The iron and steelmaking industry is currently facing several problems. For many years, it profited from using energy-dense, cheap coal. As a result, in 2023, 70.4% of the world's steel was produced using the blast furnace–basic oxygen furnace (BF–BOF) process [1]. The major drawback of this production method is its high CO_2 emissions rate, averaging at 2.32 tons of CO_2 per ton of crude steel [1]. As the result, the iron and steelmaking sector is responsible for 7%–8% of global anthropogenic greenhouse gas emissions and should therefore decrease its CO_2 emissions, ideally achieving net-zero emissions in the near future [2]. One of the main methods currently accepted worldwide is to substitute carbon with hydrogen gas (H_2) as a reductant and energy source. To realize this in practice, there is growing interest in replacing existing BFs with shaft furnaces for the solid-phase direct reduction of iron ore [3–7]. Currently, direct reduced iron (DRI) accounts for only around 10% of global iron production, 68% of which is produced using gas-based methods [1, 8]. However, this trend is set to change in the future due to government policies and investments in decarbonizing the steelmaking sector [9–12].

The BF–BOF route remains dominant in ironmaking due to its high productivity and relatively low cost of production [13]. To achieve comparable productivity in DRI production, extensive research has been devoted to the use of H_2 as a reductant in solid-state iron oxide reduction [7, 14–21]. In addition, other researchers have investigated the influence of external energy sources on physicochemical processes in reduction systems [22–24].

Ionizing and non-ionizing radiation (such as ultrasonic waves, visible light, electromagnetic fields, γ-rays, and others) has been studied by various authors for its influence on the reduction of iron oxides. Radiation has been shown to accelerate both the oxidation of metals and their reduction from oxides [25]. Studies [26–28] report significant enhancements in the reduction kinetics of iron

oxides by H_2 and carbon monoxide under ionizing and gamma radiation—either during or prior to the reaction. These enhancements often include a reduction in onset temperature and are linked to favorable changes in gas chemisorption, weakening of metal–oxygen bonds, increased ion diffusion, and facilitated phase transitions. The positive effects of γ-rays are particularly notable when used in conjunction with catalysts [27].

Ultrasonic acoustic energy also influences a wide range of physical and chemical processes. It promotes mass transfer, accelerates diffusion within solid phases, and aids structural rearrangements at the crystal lattice level [29]. In his work, Chauhan [29] showed that ultrasonic treatment increases both the oxidation of iron by air and its reduction by H_2 and carbon monoxide. These outcomes are generally attributed to intensified external mass transfer, faster diffusion, and energy dissipation at the gas–solid interface.

The impact of external electric fields has likewise been explored. Such fields can modify diffusion and electron transfer in ionic crystals and metals, thereby affecting reaction kinetics [30, 31]. Similarly, magnetic fields have been found to alter the rate of iron oxide reduction. A number of studies highlight accelerated reduction by H_2 under magnetic influence, with a lowered onset temperature, though no comparable effect is observed for CO or CH_4 [32–34]. The work by Svare (1973) linked this effect to the local enrichment of H_2 at the ferromagnetic surface [32], while Peters (1973) attributed it to an additional energy contribution from the magnetic field [33]. Nevertheless, no systematic study has been conducted on the influence of EMF on the reduction process of iron oxides.

Therefore, the aim of this study was to systematically investigate the influence of EMF on the reduction of iron oxides by H_2 under EMF application at various frequencies. To achieve this, different iron oxide materials were reduced in a thermogravimetric apparatus under controlled reducing atmospheres. Changes in the mass of the samples and gas absorbers were continuously recorded and used to analyze the reduction process.

2 | Materials and Methods

Reduction experiments were carried out using high-purity hematite (Fe_2O_3), magnetite (Fe_3O_4), and oolitic iron ore from Orken-Lisakovsk (Kazakhstan). The chemical compositions of the Orken-Lisakovsk ore is presented in Table 1. The particle sizes of the ore was in the range of 0.5–2 mm.

The reduction experiments were performed in a laboratory thermogravimetric system, the schematic of which is shown in Figure 1.

For each experiment, 5 g of iron oxide sample were placed in an alumina crucible (inner diameter 10 mm, outer diameter 30 mm). The crucible was initially positioned in the cold zone of the furnace. The furnace was then isolated and flushed with argon to establish an inert atmosphere. Heating was performed in a resistance furnace equipped with a 1 mm Ni–Cr–Fe heating element (accuracy ± 0.5 °C). The furnace temperature was raised to the target range of 673–1173 K. After reaching the set temperature, the crucible was lowered into the hot zone of the furnace and was held there for 5 min to stabilize the temperature of the furnace and to heat up the charge itself. Thereafter, the gas atmosphere was switched to a reducing consisting of pure H_2 at the controlled gas flow rate.

During the reduction process, changes in the mass of the sample (accuracy ±0.01 g) and the absorbers for off-gases were continuously recorded. These data were used to calculate the degree and rate of reduction. The degree of reduction was defined as the ratio of the oxygen removed during the reduction process to the total oxygen initially bound to iron in the sample. The average reduction rate was defined as the ratio of the total oxygen removal to the reduction time until complete reduction was achieved. The reaction was considered complete when no further change in mass was observed during a 10 min holding period. Upon completion, the furnace was flushed with argon to remove residual reducing gases, and the crucible was transferred to the cold zone for cooling under an argon atmosphere.

Experiments were performed both without EMF and with externally applied EMF. For extremely low-frequency EMF, the inductor was a multi-turn copper solenoid powered through an autotransformer, which allowed to achieve magnetic field intensity of 24 kA/m. The alternating current frequency supplied to the solenoid was adjusted using a multivibrator.

Middle-frequency magnetic field was generated using a water-cooled copper tube inductor. The inductor was powered and controlled using a UZG-5 power generator (up to 5 kW, 7–40 kHz, distortion (into 600 Ω load) up to 0.3 %) in combination with a GZ-33 master generator (up to 5 W, 20–200 kHz). The power supplied to the inductor was monitored using an indicator (scale range 0–100), while the applied voltage was measured with a tube voltmeter. The magnetic field intensity H was 432 A/m.

Because the application of EMF can cause additional heating of the sample, further experiments were conducted to evaluate this effect. To quantify the temperature rise induced by EMF, supplementary measurements were performed, comparing the temperature difference between a thermocouple placed below the crucible and another embedded within the sample. In addition, experiments using two modes of variable furnace power control were carried out:

Mode 1: Reduction under EMF with constant furnace power, allowing the sample temperature to rise due to external field effects.

Mode 2: Reduction under EMF with active furnace power adjustment, maintaining a constant sample temperature despite the EMF.

To ensure the reliability of the results, each experiment presented in this study was performed in triplicate.

TABLE 1 | Chemical composition of Orken-Lisakovsk iron ore in wt. %.

Fe_{total}	FeO	SiO_2	Al_2O_3	CaO	MgO	MnO	S	P
24.38	12.59	48.49	2.15	1.19	1.31	0.35	0.03	0.27

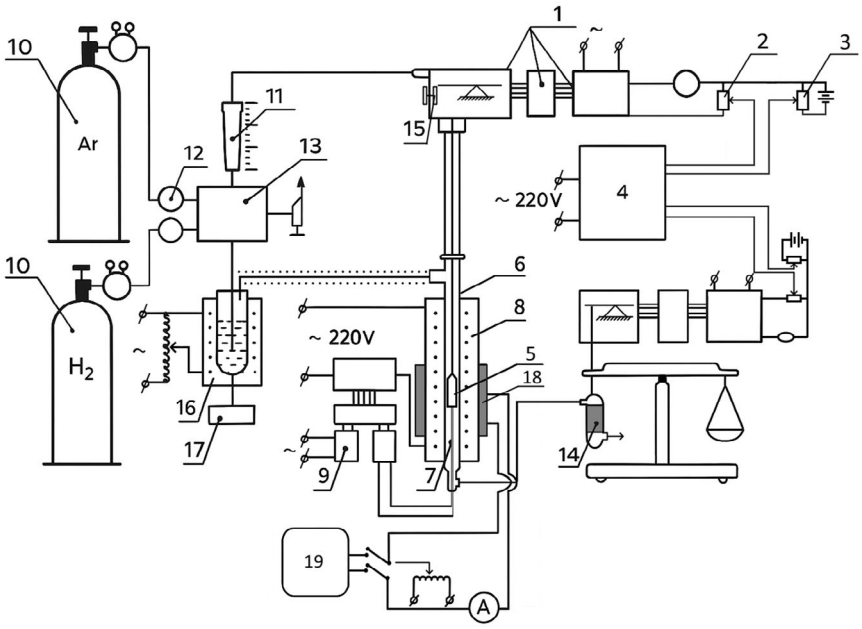

FIGURE 1 | The scheme of the experimental thermogravimetric setup 1, mechanoelectrical transducer; 2, scale divider; 3, EMF generator; 4, automatic potentiometer; 5, sample holder; 6, isolation wall of the furnace; 7, thermocouple type-B ($\Delta = \pm 0.5\%$); 8, resistance furnace; 9, temperature controller; 10, gas cylinders; 11, rotameter; 12, flow regulator; 13, valve box; 14, H_2O absorber; 15, hoist; 16, saturator; 17, type-K thermocouple ($\Delta = \pm 0.75\%$) with potentiometric device; 18, water-cooled inductor; 19, middle-frequency generator.

3 | Results and Discussion

3.1 | Effect of Extremely Low-Frequency EMF on Reduction

Extremely low-frequency EMFs ($f = 1$ to 300 Hz) are commonly used in steelmaking for melting or stirring on an industrial scale [35, 36]. Therefore, a series of experiments were conducted to study the influence of an extremely low-frequency ($f = 50$ Hz) EMF on the reduction of iron oxides in a H_2 atmosphere. The results of experiments on the reduction of high-purity Fe_2O_3 and Fe_3O_4 at an H_2 flow rate of 300 cm^3/min and a temperature of 973 K are presented in Figure 2.

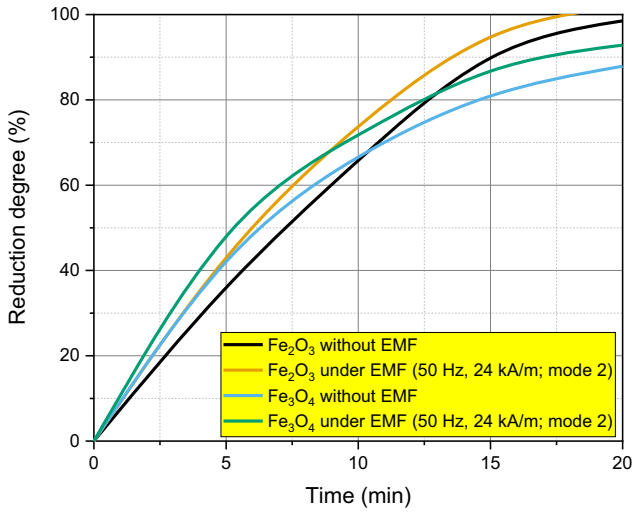

FIGURE 2 | Results of the reduction of high-purity Fe_2O_3 and Fe_3O_4 at a H_2 flow rate of 300 cm^3/min at 973 K.

The results showed that the application of an extremely low-frequency EMF to both Fe_2O_3 and Fe_3O_4 accelerated the reduction of the samples compared with the experiments conducted without EMF, with no significant difference observed between the two oxide types. After 5 min of reduction, the difference in reduction degree with and without EMF was 7% for the Fe_2O_3 sample and 5% for the Fe_3O_4 sample. After 15 min, the difference was 5% for Fe_2O_3 and ≈ 5.8% for Fe_3O_4. Therefore, high-purity Fe_2O_3 was selected for further experiments to study the effect of EMF on the reduction process, since both oxides exhibited similar responses to EMF application.

In addition, several experiments were conducted to investigate how the application of EMF influences the reduction of iron oxide under varying temperatures and gas flow rates. For this purpose, Fe_2O_3 samples were subjected to reduction both without and with the application of an extremely low-frequency ($f =$ 50 Hz) EMF over a temperature range of 773–1073 K and at H_2 flow rates ranging from 100 to 500 cm^3/min. The results are presented in Figure 3.

The results presented in Figure 3 demonstrate that increasing the temperature at which reduction takes place decreases the time required to achieve complete reduction, while increasing the H_2 flow rate enhances the reduction rate. These findings are in good agreement with those of other authors, which have shown that higher temperatures and flow rates accelerate the reduction process [14, 37, 38].

An increase in the reduction temperature by 300 K halved the time required for complete reduction in both cases—with and without EMF application. Moreover, the application of EMF significantly shortened the overall reduction time, with the most pronounced effect observed in the temperature range of 873–973 K. At 973 K, the application of EMF reduced the process

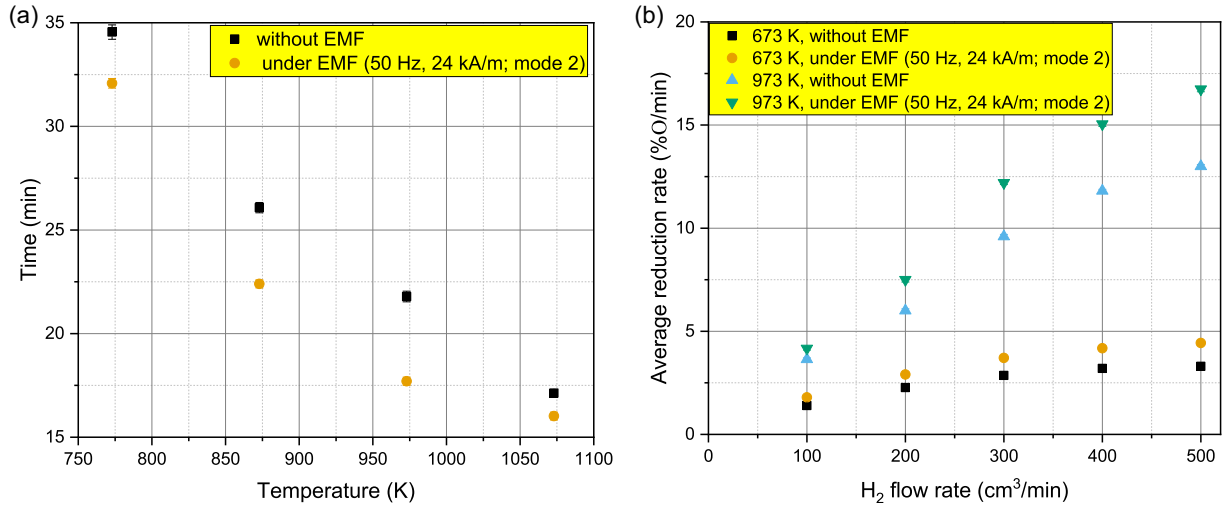

FIGURE 3 | (a) Time required to achieve a complete reduction of Fe_2O_3 at various temperatures without and under application of extremely low-frequency EMF at a H_2 flow rate of 300 cm^3/min. (b) Effect of a various H_2 flow rate on reduction of Fe_2O_3 at 673 K and 973 K.

duration by approximately 4 min. Additionally, the influence of EMF on Fe_2O_3 reduction became more significant with increasing temperature and H_2 flow rate.

It is well known, however, that the application of EMF can potentially induce additional heating of charged materials, thereby accelerating the reduction process. To examine this possibility, an additional experiment was conducted to determine whether an extremely low-frequency EMF ($f = 50$ Hz) causes measurable heating of the charge. For this purpose, a second thermocouple was inserted into the charge at 973 K, and reduction was carried out under EMF application while monitoring the temperatures from both thermocouples. No detectable temperature difference was observed when EMF was applied. Therefore, the observed acceleration of the reduction process resulting from EMF application cannot be attributed to additional heating of the material.

3.2 | Effect of Middle-Frequency EMF on Reduction

The next stage of the study was to investigate the influence of middle-frequency EMF on the reduction process of iron oxide. For this purpose, Fe_2O_3 was reduced in a H_2 atmosphere both without and with the application of a middle-frequency ($f = 25$ kHz) EMF at 673 K. The results are presented in Figure 3.

As shown in Figure 3, the application of middle-frequency EMF significantly increased the reduction degree after 20 min of reduction compared with the experiment without EMF, by ≈30%.

Similar to the experiments conducted with extremely low-frequency EMF, additional tests were performed to determine whether the application of middle-frequency EMF caused any heating of the charge. In contrast to the extremely low-frequency case, different results were obtained. Although the furnace power was kept constant, a temperature increase of ≈ 18 K at 773 K and about 8 K at 1073 K was observed in the charge, indicating that the magnitude of temperature rise decreased as the experimental temperature increased.

To further investigate this effect, reduction experiments under EMF were conducted in two different power control modes (Figure 3). Switching from Mode I (constant furnace power) to Mode II (stabilized furnace temperature) reduced—but did not eliminate—the accelerating effect of EMF on the reduction process. This suggests that the enhanced reduction degree is not solely due to additional heating of the charge. Moreover, increasing the H_2 flow rate further promoted reduction, although the effect of EMF on the reduction rate was less sensitive to flow rate than in the extremely low-frequency experiments. Nevertheless, the application of middle-frequency EMF resulted in a substantially greater increase in the reduction degree compared with extremely low-frequency EMF.

3.3 | Reduction Experiments of Industrial Iron Ores

To further confirm the positive effect of middle-frequency EMF on the reduction process of iron oxides, industrial iron ore material was used in the next stage of the study. The Orken–Lisakovsk iron ore was reduced in a H_2 atmosphere, and the results are presented in Figure 4.

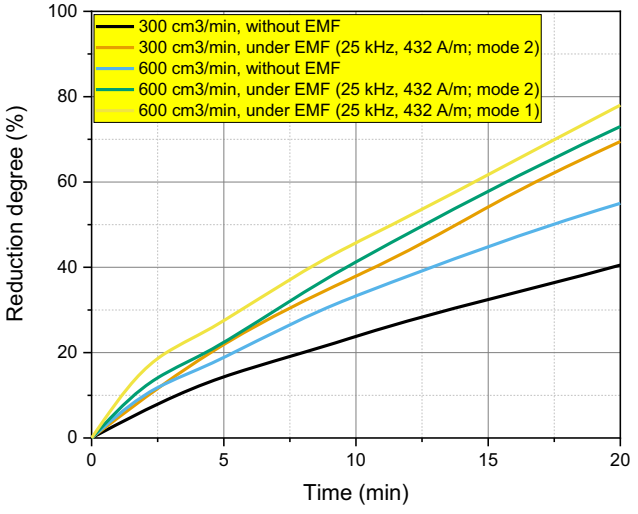

FIGURE 4 | Reduction of Fe_2O_3 at 673 K with varying H_2 flow rates and with varying power control modes.

The reduction experiments were conducted at two temperatures (973 K and 1173 K) to examine whether the magnetic properties of iron could influence the results. Overall, the application of EMF significantly accelerated the reduction process of the industrial samples. At 973 K, the reduction degree increased by 7.6% after 5 min and by 8.2% after 15 min. At 1173 K, the increase was 8% after 5 min and 4% after 10 min. As the results, effects of EMF are comparable to those observed for high-purity oxides. Notably, this effect persisted even at elevated temperatures (e.g., 1173 K), which exceed the Curie point of iron (1043 K [39]), above which iron loses its magnetic properties. Therefore, the observed results are unlikely to be explained by the magnetic behavior of iron.

Several nonthermal EMF effects may enhance hydrogen-iron oxide reduction. EMFs are known to shift adsorption equilibria and surface dipoles [40–43]. Specifically, applied fields can increase H_2 coverage on iron oxide by enhancing uptake on the substrate [44]. Furthermore, EMFs can promote spin transitions and modify electron transfer pathways during reduction [45]. By facilitating H_2 adsorption and H–H dissociation, these fields potentially assist proton diffusion or vacancy migration within the oxide lattice [45]. All these effects can lead to increased pore formation in the reducing material during the initial stages of the reduction reaction. This consequently can increase the penetration of reducing gas into the pellet at the following stages [15, 46] .

The Orken–Lisakovsk ore showed a notably high reduction degree, particularly at high temperatures. High silica concentrations typically densify the ore structure and promote the formation of low-melting silicates [14, 47]. This can result in a viscous slag phase that hinders gas-solid contact [47]. However, the experimental temperature range used in this study eliminated low-melting phase formation. Consequently, gas permeability was maintained throughout the process. Furthermore, as silica and associated silicate gangue minerals are electrical insulators characterized by a very low dissipation factor (~10^{-4}) [48, 49], EMFs penetrate the silica-rich ore with negligible attenuation (Figure 5).

These findings indicate that the application of EMF in the direct reduction of iron ore in shaft furnaces using H_2 could be beneficial. EMF accelerates ore reduction when a gaseous reducing agent is employed and, more importantly, reduces the amount of H_2 required to achieve the same degree of reduction. This is particularly significant given the high cost of H_2, which largely depends on its production method and, in particular, on the cost of electricity [50, 51].

However, transitioning this technology from controlled lab-scale experiments to large-scale industrial shaft furnaces presents a significant challenge. Industrial shaft furnaces have significantly larger diameters compared to typical laboratory TGAs. For example, widely used MIDREX shaft furnaces range from 3.7 m in diameter for prototypes to 7.15 m for the commercial furnace in Portland, Oregon [52].

Consequently, industrial shaft furnaces can suffer from the skin effect, making it challenging to maintain uniform magnetic and electric field intensities throughout the burden. The skin effect tends to concentrate induced currents on the periphery [53], creating a gradient where the outer and inner layers of the burden undergo varying degrees of reduction. While the skin effect is highly dependent on the conductive material (the burden), it can be mitigated by shifting frequencies to lower values, as current flow becomes more concentrated near the surface as frequency increases [53].

Another issue is that shaft furnaces (e.g., MIDREX or HYL) typically consist of a steel vessel lined with refractory materials. Because steel is ferromagnetic (except of austenitic steel), it would absorb the electromagnetic energy. Therefore, the vessel requires nonmagnetic construction materials, leading to increased capital investment. Furthermore, the use of induction coils generates significant waste heat, requiring active cooling systems. Moreover, the application of EMF can create a harsh electromagnetic environment capable of inducing dangerous voltages in nearby conductive structures and interfering with sensitive electronics. These factors necessitate additional mitigation costs. However, depending on market conditions, the process may become economically viable if the energy and reductant savings from accelerated reduction offset the electricity and capital costs. Therefore, a possible way to apply EMF with lower capital costs is to utilize it in the upper part of the vessel to induce pore formation.

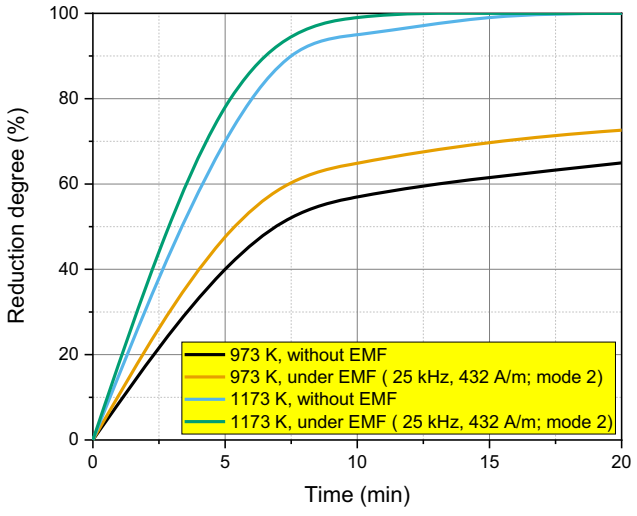

FIGURE 5 | Results of the reduction of Orken–Lisakovsk iron ore at a H_2 flow rate of 600 cm^3/min at varying temperatures.

4 | Conclusion

This study investigated the influence of EMF of varying frequencies on the reduction behavior of high-purity iron oxides and industrial iron ore in a H_2 atmosphere using the thermogravimetric method. The following conclusions can be drawn:

1. The application of both low- and middle-frequency EMF positively affects the reduction behavior of iron oxides in H_2 with the most effect observed at the early stages of reduction. This effect cannot be attributed to additional heating of the charge caused by EMF, as the results showed that only middle-frequency EMF induced a measurable temperature increase. However, this effect is negligible when furnace power is controlled, and the temperature rise decreases with increasing experimental temperature.
2. The positive influence of EMF on the reduction behavior was also observed during the reduction of industrial iron ores in H_2, confirming that this approach can be applied for industrial-relevant materials.

3. The accelerating effect of EMF on the reduction process persists at temperatures above the Curie point, indicating that the observed phenomena cannot be explained solely by the magnetic properties of iron.

Overall, the results indicate that electromagnetic field-assisted direct reduction can be observed as a promising approach to accelerate the H_2-based reduction of iron ores.

Acknowledgements

Open Access funding enabled and organized by Projekt DEAL.

Funding

The work was supported by the ESF Elbe-Stahlwerke Feralpi GmbH, project number 051201112A; the German Research Foundation (DFG), project number 461482547; and the Erasmus+ KA 171 International Credit Mobility (2023–2026).

Conflicts of Interest

The authors declare no conflicts of interest.

Data Availability Statement

The data that support the finding of this study are available from the corresponding author upon reasonable request.

References

1. *World Steel in Figures 2025*, accessed 30 July, 2025, https://worldsteel.org/data/world-steel-in-figures/world-steel-in-figures-2025/.

2. World Steel Association, *World Steel Association* (2025).

3. S. Abanades and S. Rodat, "Solar-Aided Direct Reduction of Iron ore with Hydrogen Targeting Carbon-Free Steel Metallurgy," *Renewable Energy* 235 (2024): 121297, https://doi.org/10.1016/j.renene.2024.121297.

4. F. Küster, C. Scharm, F. An, et al., "Direct Reduction of Iron ore Pellets by N_2/H_2 Mixture: In-Situ Investigation and Modelling of the Surface Temperature during Reduction Progression," *Minerals Engineering* 215 (2024): 108827, https://doi.org/10.1016/j.mineng.2024.108827.

5. D. Khasraw, C. Martin, J. Herbert, and Z. Li, "A Comprehensive Literature Review of Biomass Characterisation and Application for Iron and Steelmaking Processes," *Fuel* 368 (2024): 131459, https://doi.org/10.1016/j.fuel.2024.131459.

6. A. Gurgel, K. Benavides, J. Morris, et al., "Role of Advanced Steelmaking Technologies in Global Climate Change Mitigation Scenarios," *Journal of Cleaner Production* 513 (2025): 145726, https://doi.org/10.1016/j.jclepro.2025.145726.

7. M. Levchenko, O. Kovtun, S. Guhl, M. Gräbner, and O. Volkova, "Direct Reduction of Solid V_2O_5 with Hydrogen at 600–1400 °C," *Steel Research International* 96 (2025), https://doi.org/10.1002/srin.202300705.

8. Midrex Technologies, Inc, *World Direct Reduction Statistics 2024* (2025), 16.

9. D. Rossetto, "The Role of Border Carbon Adjustments and Subsidies in Incentivising Investment: Comparing Equivalence in the Context of Steel Recycling and Decarbonisation," *Discover Sustainability* 5 (2024): 132, https://doi.org/10.1007/s43621-024-00337-9.

10. A Green Steel Decade for China, accessed September 10 2025, https://www.climatebonds.net/news-events/blog/green-steel-decade-china.

11. Y. Zhu, Y. Hu, and Y. Zhu, "Can China's Energy Policies Achieve the "dual Carbon" Goal? A Multi-Dimensional Analysis Based on Policy Text Tools," *Environment, Development and Sustainability*. (2024), https://doi.org/10.1007/s10668-024-05190-4.

12. M. Levchenko, H. P. Markus, M. Schreiner, M. Gräbner, and O. Volkova, "Reduction of Liquid Steelmaking Slag Using Hydrogen Gas as a Reductant," *Metals* 15 (2025): 984, https://doi.org/10.3390/met15090984.

13. A. Boldrini, D. Koolen, W. Crijns-Graus, E. Worrell, and M. van den Broek, "Flexibility Options in a Decarbonising Iron and Steel Industry," *Renewable & Sustainable Energy Reviews* 189 (2024): 113988, https://doi.org/10.1016/j.rser.2023.113988.

14. O. Kovtun, M. Levchenko, M. O. Ilatovskaia, C. G. Aneziris, and O. Volkova, "Results of Hydrogen Reduction of Iron Ore Pellets at Different Temperatures," *Steel Research International* 96 (2025): 2300707, https://doi.org/10.1002/srin.202300707.

15. O. Kovtun, M. Levchenko, E. Oldinski, M. Gräbner, and O. Volkova, "Swelling Behavior of Iron Ore Pellets during Reduction in H_2 and N_2/H_2 Atmospheres at Different Temperatures," *Steel Research International* 94 (2023): 2300140, https://doi.org/10.1002/srin.202300140.

16. O. Kovtun, M. Levchenko, S. Höntsch, et al., "Recycling of Iron-Rich Basic Oxygen Furnace Dust Using Hydrogen-Based Direct Reduction," *Resources, Conservation & Recycling Advances* 23 (2024): 200225, https://doi.org/10.1016/j.rcradv.2024.200225.

17. Z. Chen, C. Zeilstra, J. van der Stel, J. Sietsma, and Y. Yang, "Review and Data Evaluation for High-Temperature Reduction of Iron Oxide Particles in Suspension," *Ironmaking & Steelmaking* 47 (2020): 741, https://doi.org/10.1080/03019233.2019.1589755.

18. Y. Bai, J. R. Mianroodi, Y. Ma, A. K. da Silva, B. Svendsen, and D. Raabe, "Chemo-Mechanical Phase-Field Modeling of Iron Oxide Reduction with Hydrogen," *Acta Materialia* 231 (2022): 117899, https://doi.org/10.1016/j.actamat.2022.117899.

19. C. Feilmayr, A. Thurnhofer, F. Winter, H. Mali, and J. Schenk, "Reduction Behavior of Hematite to Magnetite under Fluidized Bed Conditions," *ISIJ International* 44 (2004): 1125, https://doi.org/10.2355/isijinternational.44.1125.

20. D. Spreitzer and J. Schenk, "Reduction of Iron Oxides with Hydrogen—A Review," *Steel Research International* 90 (2019): 1900108, https://doi.org/10.1002/srin.201900108.

21. R. Chellan, J. Pocock, and D. Arnold, "Direct Reduction of Mixed Magnetite and Coal Pellets using Induction Heating," *Mineral Processing and Extractive Metallurgy Review* 26 (2004): 63, https://doi.org/10.1080/08827500490477612.

22. J. M. Thomas, *Principles and Practice of Heterogeneous Catalysis* (John Wiley & Sons, Incorporated, 2015).

23. C. Zhao, K. Hirota, M. Taguchi, M. Takigami, and T. Kojima, "Radiolytic Degradation of Octachlorodibenzo-p-Dioxin and Octachlorodibenzofuran in Organic Solvents and Treatment of Dioxin-Containing Liquid Wastes," *Radiation Physics and Chemistry* 76 (2007): 37.

24. Z. Chen, C. Huang, T. Zhou, and J. Hu, "Strike a Balance between Adsorption and Catalysis Capabilities in $Bi_2Se_{3-x}O_x$ Composites for High-Efficiency Antibiotics Remediation," *Chemical Engineering Journal (lausanne, Switzerland : 1996)* 382 (2020): 122877, https://doi.org/10.1016/j.cej.2019.122877.

25. K. Syed, N. Krstulović, J. Casanova-Cháfer, et al., "The Role of the Pulsed Laser Deposition in Different Growth Atmospheres on the Gas-Sensing Properties of ZnO Films," *Sensors and Actuators. B, Chemical* 382 (2023): 133454, https://doi.org/10.1016/j.snb.2023.133454.

26. M. Pospíšil and J. Topinka, "Effect of the Ionizing Radiation on the Kinetics of the Reduction by Hydrogen of NiO-Fe_2O_3 Mixed Oxides of Various Genesis," *Collection of Czechoslovak Chemical Communications* 51 (1986), https://doi.org/10.1135/cccc19861561 1561.

27. B. M. Arakelyan, P. L. Gruzin, S. T. Rostovtsev, A. A. Vasiliev, V. V. Revebtsov, and V. V. Kozlovsky, in *Phase Structure and Processes*

of Element Reduction in Solid and Liquid Systems (Izd. Nauka, 1978). 108–116.

28. M. Holmboe, *Effect of Gamma-Irradiation on the Redox States of the Structural Iron in Bentonite Clay* (Swedish Radiation Safety Authority, 2023).

29. M. Chauhan, "Corrosion Inhibition of Mild Steel in 1N H_2SO_4 by 2-amino-5-Methyl-1,3,4-Thiadiazole," *Indian Journal of Chemistry, Section A* 43 (2004): 2098.

30. R. Ubic, *Crystallography and Crystal Chemistry* (Springer International Publishing, 2024), https://doi.org/10.1007/978-3-031-49752-0

31. G. Ertl, *Reactions at Solid Surfaces* (Wiley, 2009).

32. I. Svare, "Effect of Magnetic Field on Reduction of Haematite," *Nature Physics Science* 244 (1973): 78.

33. C. T. Peters, "Accelerated Reaction Rates in a Magnetic Field," *Nature Physics Science* 244 (1973): 79.

34. Y. Jin., Y.U.H., J. Zhang., and Z. Zhao, "Effects of Magnetic Field on Reduction of CaO Containing Iron Oxides," *Acta Metall Sin* 55 (2018): 410.

35. S. Seetharaman, A. McLean, R. I. L. Guthrie, and S. Sridhar, *Treatise on Process Metallurgy* (Elsevier, 2014).

36. N.-I. R. Protection, World Health Organ (2007).

37. A. Heidari, N. Niknahad, M. Iljana, and T. Fabritius, "A Review on the Kinetics of Iron Ore Reduction by Hydrogen," *Materials* 14 (2021): 7540, https://doi.org/10.3390/ma14247540.

38. S. Li, H. Zhang, J. Nie, R. Dewil, J. Baeyens, and Y. Deng, "The Direct Reduction of Iron Ore with Hydrogen," *Sustainability* 13 (2021): 8866, https://doi.org/10.3390/su13168866.

39. N. A. Spaldin, *Magnetic Materials: Fundamentals and Applications* (Cambridge University Press, 2011).

40. J. M. Asensio, A. B. Miguel, P.-F. Fazzini, P. W. N. M. van Leeuwen, and B. Chaudret, "Hydrodeoxygenation Using Magnetic Induction: High-Temperature Heterogeneous Catalysis in Solution," *Angewandte Chemie, International Edition* 58 (2019): 11306, https://doi.org/10.1002/anie.201904366.

41. I. M. Marin, D. D. Masi, L.-M. Lacroix, et al., "Hydrodeoxygenation and Hydrogenolysis of Biomass-Based Materials Using FeNi Catalysts and Magnetic Induction," *Green Chemistry* 23 (2021), 2025–2036, https://doi.org/10.1039/D0GC03495A.

42. C. Cerezo-Navarrete, I. M. Marin, H. García-Miquel, A. Corma, B. Chaudret, and L. M. Martínez-Prieto, "Magnetically Induced Catalytic Reduction of Biomass-Derived Oxygenated Compounds in Water," *ACS Catalysis* 12 (2022): 8462, https://doi.org/10.1021/acscatal.2c01696.

43. S.-H. Lin, S. Ahmedi, A. Kretschmer, et al., "Low Pressure Amide Hydrogenation Enabled by Magnetocatalysis," *Nature Communications* 16 (2025): 3464, https://doi.org/10.1038/s41467-025-58713-6.

44. J. Zhou, Q. Wang, Q. Sun, P. Jena, and X. S. Chen, "Electric Field Enhanced Hydrogen Storage on Polarizable Materials Substrates," *Proceedings of the National Academy of Sciences of the United States of America* 107 (2010): 2801, https://doi.org/10.1073/pnas.0905571107.

45. S. Zafeiratos, G. Ulrich, J.-M. Nhut, C. Michon, and C. Pham-Huu, "Electrification of Catalytic Processes with Induction Heating: The Possible Hidden Role of Non-Thermal Magnetic Fields," *Materials Today Catalysis* 12 (2026): 100134, https://doi.org/10.1016/j.mtcata.2025.100134.

46. Y. Sun, L. Xu, H. Li, et al., "Study on Electromagnetic Characteristics and Microwave Sintering Process of Iron Oxides," *Materials Today. Communications* 43 (2025): 111757, https://doi.org/10.1016/j.mtcomm.2025.111757.

47. B. Li, D. Zhu, Z. Guo, J. Pan, C. Yang, and S. Li, "Impact of SiO_2 Content on the Hydrogen Based Direct Reduction Performance of High-Grade Hematite Pellets," *Journal of Materials Research and Technology* 37 (2025): 3777, https://doi.org/10.1016/j.jmrt.2025.06.220.

48. W. Volksen, R. D. Miller, and G. Dubois, "Low Dielectric Constant Materials," *Chemical Reviews* 110 (2010): 56, https://doi.org/10.1021/cr9002819.

49. W. Cho, R. Saxena, O. Rodriguez, R. Achanta, J. L. Plawsky, and W. N. Gill, "Effects of Sintering on Dielectric Constants of Mesoporous Silica," *Journal of Non-Crystalline Solids* 350 (2004): 336, https://doi.org/10.1016/j.jnoncrysol.2004.07.084.

50. Hydrogen in Iron and Steelmaking: Ore-Based Metallics & Carbon-Neutral Steel,- accessed September 10 2025, https://www.midrex.com/tech-article/hydrogen-in-iron-and-steelmaking-ore-based-metallics-carbon-neutral-steel/.

51. Y. Ji, Z. Chi, S. Yuan, et al., "Development and Application of Hydrogen-Based Direct Reduction Iron Process," *Processes* 12 (2024): 1829, https://doi.org/10.3390/pr12091829.

52. *Midrex Technologies Inc.*, (2018).

53. W. H. Hayt Jr, *Engineering Electromagnetics*, 5th ed., (McGraw-Hill international edition, 1989).